Single Event Effect Testing with Ultrahigh Energy Heavy Ion Beam

Maria Kastriotou, Pablo Fernandez-Martines, Rubén García Alía, Carlo Cazzaniga, Matteo Cecchetto, Andrea Coronetti, Giuseppe Lerner, Maris Tali, Nourdine Kerboub, Vanessa Wyrwoll, Johannes Bernhard, Salvatore Danzeca, Véronique Ferlet-Cavrois, Alexander Gerbershagen, and Henry Wilkens

***Abstract*—Single event effect (SEE) testing with ultrahigh energy (UHE) heavy ions, such as the beams provided at CERN, presents advantages related to their long ranges with a constant linear energy transfer value. In the present work, the possibility to test components in parallel is being examined, and results from the CERN 2018 UHE Pb test campaigns are studied. Furthermore, the generation of multibit upsets by the UHE Pb ions is evaluated, and the contribution of possible fragments to the SEE measurements is discussed.**

***Index Terms*—Dosimetry, ion beams, ion beam applications, lead, radiation effects.**

I. Introduction

SINGLE event effect (SEE) testing with heavy ions is a standard technique for the qualification of electronic components, typically carried out in accelerator facilities providing ions of energies of the order of 10–20 MeV/nucleon [1], [2], which will be thenceforth referred to as standard ion energies for irradiation testing [3]. Among the advantages of these facilities, such as RADiation Effects Facility (RADEF) [4], [5] and Université Catholique de Louvain (UCL) [6], is their versatility in ion species and as a result linear energy transfer (LET) values. This renders the estimation of the SEE rate for a component in a particular radiation environment possible through the evaluation of the SEE cross section with respect to the LET in the mentioned facilities, and the subsequent folding of this function with the expected LET spectrum at the environment of interest [7].

The main challenge of testing with ions of standard energies is introduced by their relatively short ranges, of the order of up to 200 μm in silicon for the high-LET ions. Components need to be delidded, and tests are usually performed in vacuum to ensure that ions arrive to the sensitive volume. However, this opening process may be hazardous for the component, very costly or even impossible in the case of modern technologies with increased structural complexity [8]. In some facilities, the LET value of ions with short ranges may not remain constant through their passage into the sensitive volume of a component. As a result, components packaged in flip-chip have to be thinned down to about 50 μm, or multichip modules should be repackaged in planar configuration [9], [10].

Ions of very-high energy (0.1–5 GeV/nucleon) and ultrahigh energy (UHE) (5–150 GeV/nucleon) constitute an asset to heavy ion testing: due to their much larger range, they allow for the testing in air and without part delidding, while they maintain the same LET while crossing the sensitive volume of interest. In the context of radiation environments, very high energy and UHE ions are commonly found in space, such as the galactic cosmic rays of which they consist a large fraction [3], and in high energy accelerators such as the CERN Large Hadron Collider (LHC) [11].

Facilities with very-high energy heavy ion beams include GSI Helmholtzzentrum für Schwerionenforschung GmbH (GSI) [12] and NASA Space Radiation Laboratory (NSRL) [13]. The SEE phenomena at very high energies have been investigated in [9] and [14]. Heavy ions with UHEs can be found at CERN during its heavy ion experimental program. The first such test campaigns took place in 2017 and 2018, and the first results from the 2017 test campaign, as well as an analysis of the physical principles behind the observed phenomena, are summarized in [3] and [15]. The present work contains considerations on the heavy ion beam purity, and the implication of this may introduce SEE testing. Furthermore, the possibility of parallel board testing with UHE heavy ions will be examined. Finally, experimental results from both test campaigns with static random-access memory (SRAM) memories are presented, and the generation of multibit upsets (MBUs) by UHE heavy ions will be studied.

II. CERN UHE Heavy Ion Beams

The CERN accelerator complex is a combination of multiple accelerators which act as injectors to the most energetic collider worldwide, the LHC. The core scientific program of the LHC includes the collisions of protons, however, heavy ions are also employed to reach UHEs up to many TeVs and collide at the LHC experiments. The CERN heavy ion program normally takes place at the end of each calendar year and lasts approximately four weeks. Each year, a single ion species is being accelerated, commonly lead. Since 2017, the CERN UHE heavy ion beams have been used and benchmarked

This study has received funding from the European Union's Horizon 2020 research and innovation programme under the MSC grant agreement no. 721624.

Maria Kastriotou, Pablo Fernandez-Martinez, Rubén García Alía, Matteo Cecchetto, Andrea Coronetti, Giuseppe Lerner, Maris Tali, Nourdine Kerboub, Vanessa Wyrwoll, Johannes Bernhard, Salvatore Danzeca, Alexander Gerbershagen, and Henry Wilkens are with CERN, 1211 Geneva, Switzerland (e-mail: maria.kastriotou@stfc.ac.uk).

Carlo Cazzaniga is with the ISIS Facility, STFC, Rutherford Appleton Laboratory, Didcot OX11 0QX, U.K.

Véronique Ferlet-Cavrois is with the European Space Agency, ESTEC, 2200 AG Noordwijk, The Netherlands.

TABLE I
ION SPECIES, TOTAL ENERGY AND VOLUME-EQUIVALENT LET VALUES DURING THE 2017 AND 2018 CERN UHE HEAVY ION TEST CAMAPIGNS.

	CHARM		SPS-NA	
	2017 ^{129}Xe	2018 ^{208}Pb	2017 ^{129}Xe	2018 ^{208}Pb
Energy (GeV/nucleon)	6.38	5.49	19-75	150
Volume eq. LET (MeVcm^2/mg)	3.6	8.0	3.7-3.9	8.8

for SEE effect testing. In this article, results from the 2017 (xenon), and 2018 (lead) runs are discussed.

The experiments took place at the CERN high-energy accelerator mixed-field (CHARM) facility, and the Super proton synchrotron North experimental area (SPS-NA). The former is typically operated as a mixed field facility receiving beam from the CERN proton synchrotron (PS), while the latter is from the following accelerator chain, the SPS. The beam energies for the ion runs of the two years in the two facilities are summarized in Table I, together with the corresponding volume equivalent LET as defined in [3], and further discussed in Section III.

A. CHARM

CHARM is a mixed radiation field facility dedicated to the testing of electronic components, which is described in detail in [16]–[18]. Typically operating with protons, different target configurations are employed to generate a mixed radiation field in the facility. In addition, tests with the primary PS beam are possible by removing the target. The first use of the primary heavy ion beam at CHARM, including a detailed description of the facility and the beam calibration for 2017, is described in [15]. Among the beam characteristics, the intensity reaches up to 108 ions/spill while the beamline is operated with a slow extraction beam which results in a spill length of approximately 200 ms. The spill periodicity is subjected to the PS operation requirements but typically ranges from 20 to 40 s.

The instrumentation available on this beamline to characterize the beam is well suited for a typical high-intensity proton beam, but was not initially calibrated for the heavy ion case. Therefore, several calibration runs were performed at the beginning of each test campaign to obtain a calibration factor which gives the xenon and lead ion intensity at the test position out from the readout of the beam instrumentation. The calibration accuracy is affected by the uncertainties in the ion extraction from the PS, and the instruments resolution for ions. Transmission along the beamline, i.e., the ratio of the beam intensity at the device under test (DUT) location over the extracted beam intensity, is one additional parameter affecting the beam calibration factor. Taking into account the errors of the calculation, and the beam fragmentation and attenuation that may be introduced from the beam instruments and the machine elements, we considered a 20% error to cover all possible scenarios.

For the measurement of the beam size, a multiwire proportional chamber, which is located downstream from the CHARM beamline, and the DUT position, is employed. During the runs of the 2018 ion test campaign, the beam size alternated in full-width at half-maximum (FWHM) between 3 and 8 cm, depending on the experimental requirements. Combining the intensity provided by the beam instrumentation, the ion fluence in standard units of ions/cm^2 can be calculated.

B. SPS-NA

The beam of ^{208}Pb fully stripped ions is extracted from the SPS accelerator with an energy of 150 GeV/nucleon, to arrive at the SPS-NA. The setup for electronics irradiation was located in the experimental zone 138 of the experimental hall called EHN1, using the beam of the H8 beamline. The target, which is normally used during the proton runs to create pion or muon beams, had been moved out of the beam trajectory.

The beam extraction has been performed during an approximately 10 s flat top interval (called spill) of the 45-s-long SPS supercycle. The beam intensity during the 10 s extraction was comparably constant, amounting 10^3–10^5 lead ions per spill at the experimental zone. A dedicated beam optics setting has been developed in order to satisfy the beam size and uniformity requirements at the experiment location. The optics setting as well allowed to flexibly adjust the beam intensity with help from the collimators located in the first 200 m of the beamline, hence being far enough from the experimental setup in order to not contaminate the Pb beam with lighter ion fragments. The SPS-NA is also described in detail in [3].

A specially designed support consisting of aluminum frames and plexiglass plates guarantees an accurate alignment of the DUTs when placed in parallel to each other. The boards containing the DUTs can be either mounted directly on the aluminum frames, or on 4-mm-thick plexiglass plates attached to them. The center of the frames, where the DUTs are located, was aligned with the beam center in the beginning of the test campaign using a laser alignment system. A two-axis movable table was used for small corrections in the alignment.

For the beam characterization at the experimental location, two detectors are employed, a scintillator coupled to a photomultiplier, and a delay wire chamber (DWC). The former is used to measure the number of beam particles, while a pulse height analysis (PHA) function gives an estimation of the beam composition and the contaminants produced by the in-beam elements in the beam extraction line. The latter provides us with the horizontal and vertical profile of the beam. The output of the two detectors was used in a spill by spill analysis of the horizontal and vertical FWHM of the beam, as well as the number of particles that are contained in a 2 × 2 cm^2 surface (typically representative of the irradiated components), considering a bi-Gaussian transverse beam profile.

III. SEE CAUSED BY UHE HEAVY IONS

When performing SEE measurements with UHE heavy ions, one needs to take into consideration their very different energy regime compared to ions traditionally used, which can affect the interpretation of the experimental results.

The first aspect to be considered, and most relevant to the present work, is related to the structure of the UHE heavy ion

TABLE II
SEU COUNTS DURING PARALLEL TESTING OF ESA SEU MONITORS WITH THE UHE HEAVY ION BEAM.

Intensity	Irradiation duration	ESA mon 1 counts	ESA mon 2 counts	ESA mon 3 counts
Medium	00:55	3052	2549	2161
High	02:10	44127	37341	31405

ionization path, which differs compared to ions of standard energies. For the latter, the delta rays produced have a range of the order of micrometers; therefore, the energy deposition of the particle is concentrated along the particle trajectory. On the other hand, UHE heavy ion beams transfer higher energies to the delta rays, which can then trigger further ionizations in a broader volume around the ion track. Hence, the results of SEE testing with ions of UHE and standard energy are not directly comparable in terms of standard LET values. To that end, the principle of volume-equivalent LET has been defined as the average energy deposition distribution, normalized to a generalized sensitive volume of 1 μm^3, and is discussed in detail in [3], where its calculation from simulations is demonstrated.

For the ultra high ion energies discussed in this work, the volume-equivalent LET is 50%–55% of the total, unrestricted LET. This implies that for the same testing ion, less energy is deposited in the sensitive volume of the irradiated devices, potentially affecting the SEE production. The calculated values for the 2017 xenon and 2018 lead beams are summarized in Table I.

The second aspect that needs to be taken into consideration during UHE heavy ion testing is the impact of nuclear reaction products on the production of SEEs, which is also explained in detail in [3]. These products have been identified as the main source of proton- and neutron-induced SEEs through indirect energy deposition. For heavy ion tests, they are typically not considered due to the dominance of direct ionization, and the relatively low probability of nuclear reactions. However, due to the lower LET values and larger range, they became more relevant when the UHE regime was considered.

IV. SEE TESTING UHE HEAVY IONS

A. Beam Attenuation During Parallel Board Testing

The possibilities of in-air and parallel board testing comprise the major advantages of UHE heavy ion beams. The main challenge they introduce, however, is their tendency to fragment. Therefore, the careful characterization of the beam purity is crucial when evaluating components under such beams. In this section, the UHE heavy ion beam alteration during parallel board testing is examined through measurements performed with the 2018 lead beam, and respective simulations.

The basic tool for these measurements has been the reference European Space Agency (ESA) single event upset (SEU) monitor. This is a 16 Mb, multichip SRAM module, comprising four dies, and covering an area of 19.8 × 19.8 mm^2. Designed for space applications, the ESA monitor is radiation hardened, and immune to MBUs [19]–[22].

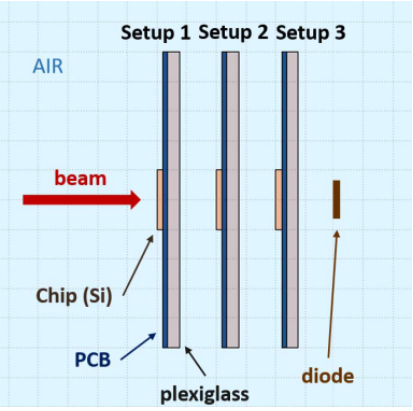

Fig. 1. Experimental setup simulated with FLUKA.

Three identical reference ESA SEU monitors were installed in parallel in the SPS-NA, each mounted on one plexiglass plate (setup 1, 2, and 3, from the closest to the furthest to the beam), as shown in Fig. 1. The monitors were irradiated with Pb beams of three different initial intensities, low (10^3 particles on the scintillator), medium (10^4 particles on the scintillator), and high (10^5 particles on the scintillator) per spill. The FWHM of the beam was approximately 3.4 × 3.4 cm^2 in all cases. The results of this study in terms of SEU counts are summarized in Table II.

A Monte Carlo simulation with the particle transport code FLUKA [23], [24] was performed in order to further evaluate the experimental results. The designed geometry, shown in Fig. 1, consists of three setups in parallel, each including the 4-mm plexiglass frame, an 1.5-mm printed circuit board (PCB), a 34-μm copper layer on its surface, and a 2-mm chip made of silicon. The simulated beam, consisting of Pb ions with a 150-GeV/c/nucleon energy, was narrow, with a 0.5-cm FWHM in both x and y dimensions and starting only 0.5 cm ahead of the first chip in order to increase the calculation statistics. The resulting primary beam attenuation introduced by each of the first two setups to the primary beam impinging onto them, for both the experiment and simulation, is summarized in Table III. For the nth setup the attenuation attn it introduces to the beam was calculated as:

$$att_n = (x_n - x_{(n+1)})/x_n \quad (1)$$

where the value x_n corresponds to the SEU counts of the nth monitor in the experimental case, and to the number of primary beam particles that impinge on the chip of the *n*th setup in the simulations. It can be noted that the simulations and the experimental data for the cases of both medium and high intensity are in very good agreement, and in every case, each setup seems to introduce an attenuation of 15%–17% to the primary beam.

It should be noted at this point that a major part of the beam attenuation is being introduced from the plexiglass plate holding the board. When repeating the simulation without the plexiglass plate in setup 1, the attenuation after the first setup falls to 7.5% of the primary beam.

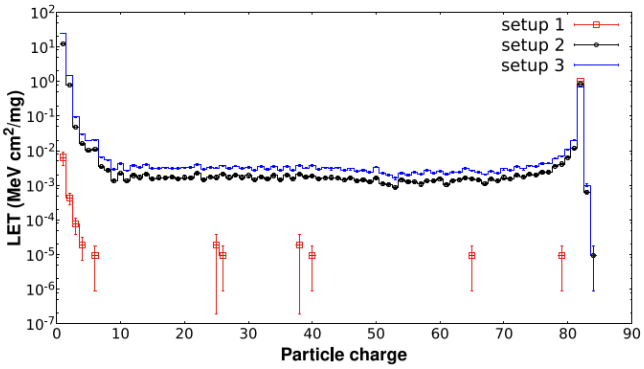

Fig. 2. Distribution of particles before setup 1–3, as a function of their charge, per primary beam particle simulated to impinge on setup 1.

TABLE III
ATTENUATION INTRODUCED TO THE UHE HEAVY ION BEAM BY EACH SETUP, DURING PARALLEL BOARD TESTING.

	Medium	High	FLUKA
Setup 1	16.5%	15.4%	15%
Setup 2	15.2%	15.8%	17%

In Fig. 2, the charge distribution of particles according to their charge impinging on setup 1–3 can be observed, per primary lead particle, as this was calculated in the same simulation. The attenuation is defined as the reduction in the number of particles with Z = 82, which corresponds to the primary beam.

B. Consideration on Beam Purity

A detailed understanding of the beam purity is crucial for a successful SEE testing. While traveling through a beam line, the heavy ion beam is usually considered to be pure, as any secondary particles produced are being discarded by the magnetic elements. However, as these beams can be easily fragmented, any intercepting element may introduce secondary particles.

In the 2018 SPS-NA heavy ion experiments, we examined in detail the beam purity while testing with the 150 GeV/c/nucleon momentum Pb ions. In particular, following the window of the vacuum pipe which provides the beam, different elements intervene between this and the position where SEE testing is taking place. From the beam pipe to the irradiation location, these are the scintillator, the DWC, a scintillating fiber monitor, and one diode setup.

The PHA analysis of the scintillator could already provide an estimation of the beam purity at the position of the instrument. This was defined as the number of counts in the energy deposition peak divided by the total number of counts, and was calculated at 70%. However, both the scintillator itself and the following instruments are expected to produce secondary fragments and attenuate the beam. To assess the number of ions arriving to the DUTs, the output of a silicon detector tested on the test bench was used. This diode [25] has a surface of 2 × 2 mm^2 and the ability to distinguish between the primary particles (Pb ions) and the produced

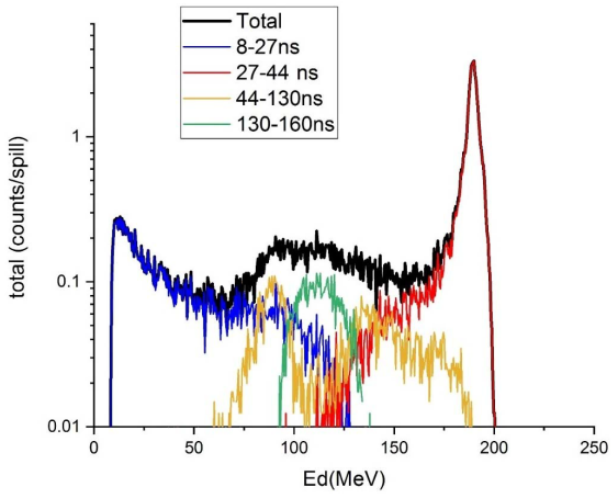

Fig. 3. Energy deposition spectra for signals with different fall times.

secondaries according to the magnitude and time structure of the deposited energy. During the experimental test, the silicon detector was installed at the fourth position of the experimental setup, behind three ESA SEU monitors, and their plexiglass supports.

The pulse shape discrimination on a solid-state detector can be achieved [26] by using a current broadband preamplifier [27]. In this case, the analysis is done using the fall time of the detector charge signals [28]. The details of this measurement, that is novel for the UHE range of the particles, will be presented in a separate publication [29]. Fig. 3 shows the energy deposition of the particles crossing the diode during a medium intensity run, and their fall time. The primary particles consist the largest energy deposition peak, and are characterized by a fall time between 27 and 44 ns, while the rest of the particles are the detected secondaries.

Using the scintillator and the beam profile information during the experiment, the number of particles that impinge on the diode were extrapolated. The diode output provides us with the number of primary particles in this beam, C_D^{prim}. Furthermore, the number of scintillator counts that correspond to an area equal of that of the diode was calculated as $C_{Sci,D}$. Considering an average of 15% of attenuation for the primary beam after traversing each of the three test board setups, as this was described in Section IV-A, the percentage of primary lead ions impinging on the first DUT α_{prim} was estimated from the following equation:

$$\alpha_{prim} = \frac{C_D^{prim}}{(1-15\%)^3 C_{Sci,D}} \quad (2)$$

This study was repeated for different runs, and primary beam was estimated as only α_{prim} = (13.5% ± 3.9%) of the initial (total) scintillator counts, where 3.9% is the standard deviation of the sample. This implies that the primary beam was highly attenuated by all the materials interposed between the DUT and the scintillator, and, to a certain extent, by the scintillator itself.

To confirm this percentage, a second analysis with a differ-

ent experimental setup was performed. In this case, the first setup comprises only a PCB board. The second setup consists of a board mounted on a plexiglass, and the third setup is an ESA SEU monitor, also mounted on a plexiglass. The silicon detector occupies the last position of the setup. Similar to the above case, the total number of particles impinging on the diode was extrapolated, and from the diode output the number of primaries in this signal was retrieved.

As mentioned in Section IV-A, the FLUKA simulations give an estimation of 7.5% for the beam attenuation due to only one board without the plexiglass plate. Considering such an attenuation for the first setup, and 15% for the following two setups, which include also the plexiglass plate, the percentage of primary beam in front of the first DUT of this experimental case was calculated as $\alpha_{prim}^{noplexi}$ = 17%, which satisfactory agrees with the previously calculated α_{prim}.

This analysis was repeated in order to estimate the amount of secondaries that arrive to the first DUT, and therefore, obtain a good characterization of the beam composition. To that end, the diode counts corresponding to fragments were compared to the extrapolated to the detector surface scintillator counts for various experimental runs. The number of nonprimary beam particles detected correspond to α_{sec} = (27% ± 10%) of the scintillator counts. The error value was set at 10% to cover the variability observed in the different runs.

Therefore, at the particular experimental setup, only 40.5% percent of the scintillator counts arrive to the fist DUT. Of that percentage, one-third is primary beam, and the rest secondaries. The severe attenuation of the beam is attributed to the many beam instruments intervening between the window of the beam pipe and the DUTs, as well as the large in-air distance (approximately 2 m) between the two.

V. Measurements of SEEs with UHE Heavy Ions

A. SEU Measurement with ESA Monitor

A variety of electronic components and different setups were irradiated during the UHE ion campaigns at CERN. Among them, the ESA SEU reference monitor was irradiated in all the facilities. In Fig. 4 the SEU cross sections measured with both the CERN UHE ion beams, together with those measured at other ion facilities of standard and very high energies, are presented. As explained in Section III, the volume-equivalent LET is being used for the UHE beams. The values measured for xenon are discussed in [3] and [15]. In the case of lead, the CHARM irradiation resulted in a cross section of $\sigma_{Pb,CHARM}$ = (6 ± 4.2) × 10^{-9} cm^2/bit. The high error in this case is related with the uncertainties in the beam transmission during the different runs, resulting in a 30% uncertainty set for the beam intensity. At the SPS-NA, the calculated cross section is $\sigma_{Pb,NA}$ = (1.6 ± 0.3) × 10^{-8} cm^2/bit. In this case, the error is smaller due to the detailed knowledge of the beam characteristics.

It can be observed that the measured SEU cross section in the case of the SPS-NA Pb beam is roughly two times the value that was measured in other facilities. However, this cross section has been calculated for only the primary beam, which as described in Section IV, is approximately one-third of the

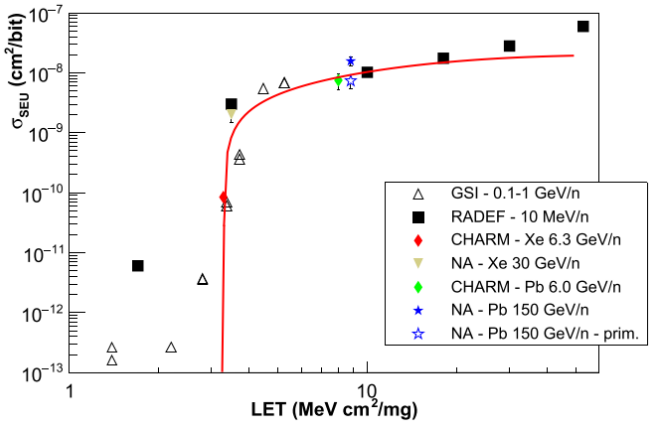

Fig. 4. SEU cross section of the ESA SEU monitor, as measured in very- (GSI) and ultrahigh (CERN) energy heavy ion beams, and in RADEF. The Weibull fit of the datapoints has been superimposed. In the case of the 2018 SPS-NA beam, the calculated value of the contribution of only the primary beam has been added.

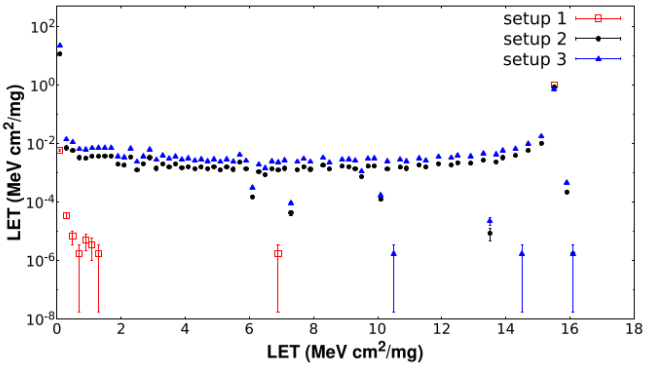

Fig. 5. Unrestricted LET distribution of particles right before setup 1–3, per primary beam particle simulated to impinge on setup 1.

total particles impinging on setup 1. This implies that a large amount of different particles with variable LET values also reach the SEU monitor. Even though the primary beam has the highest LET and is the main contributor to the SEEs of a DUTs, these particles may also trigger SEUs which will increase the cross section value. In Fig. 5 the unrestricted LET distribution of particles when 150 GeV/c/nucleon beam impinges on setup 1, right before setup 1, 2, and 3 is presented, and confirms the fact that the primary beam is expected to have the highest LET compared to the generated fragments.

B. Weibull Fit

The measured cross sections of the ESA SEU monitor under the CERN UHE heavy ion beams with respect to their volume-equivalent LET value are presented in Fig. 4. In the figure, the datapoints from measurements in GSI, with very high energy (0.1–1 GeV/n) Nickel beam have been added, as well as datapoints from measurements with different ions in RADEF [9]. To estimate the LET for the former case, Stopping and Range of Ions in Matter (SRIM) [30] was used and the tabulated LET was compared to the volume equivalent one,

TABLE IV
WEIBULL FIT PARAMETERS FOR THE ESA SEU MONITOR CROSS SECTION TO UHE HEAVY IONS.

σ_{sat} cm^{2}bit^{-1}	L_0 MeVcm^2/mg	w MeVcm^2/mg	s
$(2 \pm 0.9) \times 10^{-8}$	3.3 ± 0.1	8.7 ± 6.3	0.65 ± 0.2

as calculated using FLUKA. The values of the two methods agree for the energies of some hundreds of MeV/nucleon, and therefore, for the particular ion at these energies and target, the energy deposition does not exceed the micrometric volume of the particle track. For higher energies, the volume-equivalent LET, calculated with FLUKA, was used.

The cross section of SEUs with respect to the LET can be represented by a Weibull function:

$$\sigma = \sigma_{sat}\left(1 - e^{\left(\frac{L-L_0}{w}\right)^s}\right) \quad (3)$$

where σ_{sat} is the saturation cross section (in cm^2/bit), L_0 is the onset LET, s is the shape and w is the width parameter of the Weibull function. The ESA monitor data were fit with this function using the ROOT [31] data analysis framework, while the datapoints of the sub-LET threshold region (LET values lower than 2.5 MeVcm^2/mg) were ignored. As discussed in [32], the sub-LET threshold regions cross sections are significantly dependent on the ion energy, which in the presented experiments varies by many orders of magnitude. The resulting curve was found to nicely fit the experimental data, therefore, was used later in Section VI. The estimated fit parameters are summarized in Table IV.

C. SEUs and MBUs on SRAMs

Two additional memories were examined for SEUs at the 2018 test campaign at the SPS-NA. One is a 65 nm technology, 32 Mbit SRAM from ISSI, the IS6164WV204816BLL, and the other a 90 nm technology, 8 Mbit SRAM from Cypress, in particular, the CY62157EV30LL-45ZSXI. For the testing of the two memories a generic SRAM tester developed at CERN and described in detail in [33] and [34], the CERN SEU Tester, was used. The memories were irradiated perpendicularly to the beam, and with a tilting angle of 60°. In the second case, the effective LET, LET_{eff}, of the beam particles is calculated as:

$$LET_{eff} = \frac{LET_{vol.eq.}}{cos\theta} \quad (4)$$

where θ = 60° is the tilting angle.

The data from the memories were further analyzed for MBUs, which have not been observed under standard energy ion irradiation. The assumption behind this analysis was that the broader particle tracks of the UHE heavy ions may result to more than one bit flips. It should be noted here that the irradiation of the same setup in RADEF did not result in any MBU generation.

The experimental results obtained in the SPS-NA are summarized in Table V. The SEU cross section is higher in the case of the 60° tilt, due to the higher effective LET, i.e., the longer distance that the particle is crossing in the sensitive volume of the component when the path of the ion is not normal to the surface of that volume. From the acquired data, no connection between the very high energy of the heavy ions and the generation of MBUs can be made. However, one may notice one case of an MBU with a multiplicity of 2, in the case of the Cypress memory tilted at 60° with respect to the beam axis. This may be an indication that indeed, very high energetic particles may result in a broader ionization track that will lead to MBUs, however, more experiments and longer irradiation times are required to confirm this. Moreover, due to memory scrambling and interleaving, the absence of MBUs does not rule out possible multicell upsets (MCUs) that may be happening in adjacent SEU cells belonging to different words.

TABLE V
SEU AND MBU RESULTS OF THE ISSI SRAM UNDER UHE PB IRRADIATION.

Memory	Effect	0° 8.8 MeVcm^2/mg	60° 17.6 MeVcm^2/mg
ISSI	SEU	421	393
	σ_{SEU} (cm^{2}bit^{-1})	2.83×10^{-9}	9.70×10^{-9}
	MBU	0	0
Cypress	SEU	447	720
	σ_{SEU} (cm^{2}bit^{-1})	2.2×10^{-8}	1.01×10^{-7}
	MBU	0	1

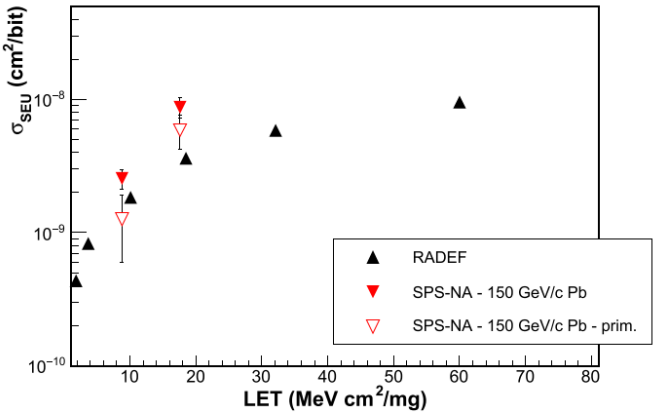

Fig. 6. SEU cross section of the ISSI memory at the CERN UHE Pb and RADEF standard energy heavy ion beam.

In the case of the ISSI SRAM, the SPS-NA results have been compared with data acquired at RADEF, with different heavy ions and different LETs, as presented in Fig. 6, in which the former are represented by full point-down, and the latter by point-up triangles. It can be observed that the cross sections measured with the CERN UHE Pb beam are higher than the ones measured in RADEF. This difference stems from the contribution of secondary particles to the final SEU measurement, as will be discussed in Section VI.

VI. CHALLENGES IN BEAM PURITY AND CONTRIBUTION OF SECONDARIES WHEN TESTING WITH UHE HEAVY IONS

The beam purity during heavy ion testing, which is a result of the in-air testing and the interference of beam diagnostics

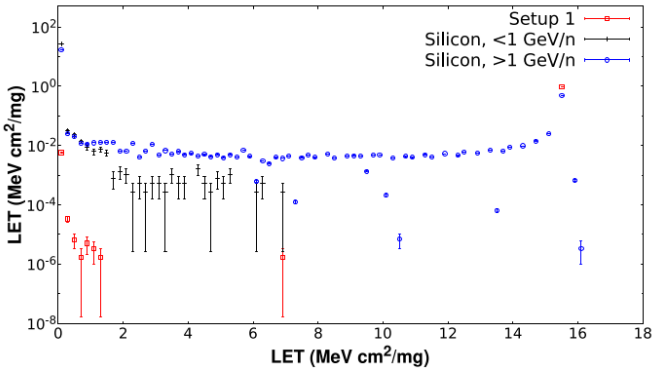

Fig. 7. LET distribution of a 150 Gev/c/nucleon beam, before interacting with the first board setup and when arriving to the fourth board setup (silicon detector), per primary beam particle. The contribution at the fourth board has been disentangled to very high energy and UHE particle contribution, and to particles with energies lower than 1 GeV/c/nucleon.

equipment, should be taken under consideration when performing SEE estimations. In particular, the understanding of the composition of the beam including the secondary particles is of high importance.

In Section IV-B the composition of the SPS-NA UHE Pb beam has been carefully estimated. Only 40.5% of the particles measured by the scintillator arrive to the first DUT, one-third of which is primary ion beam while the rest (α_{sec} = (27% $\pm$ 10%) of the scintillator counts) are secondaries.

The distribution of these particles with respect to their unrestricted LET value is presented in Fig. 5. The figure shows the LET of the beam before interacting with the DUTs, in front of setup 1, which consists as expected of a very high peak at the primary beam LET value. After crossing two setups and before the third, a large amount of secondary particles have been generated. The LET distribution of the secondary particles peaks at very small values (which do not contribute to the SEE generation) and has a second peak at the primary beam LET. Between them, a valley of almost equiprobable values is observed. Such a distribution is expected when the primary beam transverses any type of structure and material, including the beam instrumentation devices. As a result, this LET distribution represents also the one expected in front of the first DUT of the experiment, when the beam has crossed these devices.

In order to correctly estimate the contribution of these fragments to the measured cross section, it is important to evaluate if these are of very/ultrahigh or lower energies, and therefore, if they are represented by their unrestricted or volume-equivalent LET values. To that end, the geometry of Fig. 1 was repeated, with a fourth setup simulated 2-cm downstream and representing the diode, and a 150 GeV/c/nucleon Pb beam impinging on setup 1. Another scoring was added to the simulation, examining if the particles arriving to the last setup are of energies higher than 1 GeV/n or not. The results of this simulation are presented in Fig. 7. From the simulation it can be concluded that the majority of the secondaries created by an UHE heavy ion beam are particles with energies greater than 1 GeV/n. As described in [3], for such high energies and for SEE testing the volume-equivalent LET should be considered, which can be approximated as half of the unrestricted LET. Therefore, in order to estimate the contribution of the fragments to SEEs, their distribution is considered to be uniform for all LETs up to 8.8 MeVcm^2/mg, which is the unrestricted LET of the primary beam.

This distribution P_{sec}(LET) was integrated in ranges of 1 MeVcm^2/mg with the Weibull fit for ions σ_{ion}(LET) as:

$$\sigma_{sec} = \int P_{sec}(LET)\sigma_{ion}(LET)dLET \tag{5}$$

to provide us the integrated cross section of the secondaries σ_{sec}. For the ESA SEU monitor, Weibull function with the parameters estimated in Table IV was used, while for the ISSI the Weibull function parameters have been estimated in [34] as σ_{sat} = 1.14 × 10^{-8} cm^2/bit, E_0 = 0.2 MeVcm^2/mg, w = 40 MeVcm^2/mg, and s = 1.2. The secondary particles lead to a contribution to the total cross section of σ_{sec}. From this cross section, the SEU counts that correspond to the secondaries have been calculated as:

$$SEU_{sec} = \sigma_{sec} c_{Sci} \alpha_{sec} n_{bits} \tag{6}$$

where c_{Sci} are the counts of the scintillator, α_{sec} the percentage of these counts that corresponds to secondaries, and n_{bits} the number of bits of the memory of interest. The secondary SEU counts were removed from the total number of SEUs measured during the experiment, resulting in the number of SEUs generated by the primary beam, from which the cross section of the primary UHE heavy ion beam σ_{prim}, was calculated. This analysis was performed for the ESA SEU monitor and the ISSI SRAM, and is presented in Figs. 4 and 6, respectively.

In the case of the ESA monitor, the cross section of the primary beam was calculated as σ_{prim}^{ESAmon} = 7.32 × 10^{-9} cm^2/bit, and therefore, approximately 50% of the measured value. It can be observed that the produced value is in better agreement with the rest of the datapoints when compared to the experimentally measured cross section. It should be noted that the beam is mainly composed of fragments rather than primary ions. The contribution of the former is nonnegligible, however, the primary beam remains the main contributor to the total SEU count.

In the case of the ISSI memory, the contribution of the secondaries is also nonnegligible, and greater than 50% of the generated SEUs. This behavior is a result of the low LET threshold of the memory (estimated 0.20 MeVcm^2/mg from [34]), and the high SEU cross section for even low LET values, which result in a significant contribution of the fragments. It should be noted here that in the given case the secondaries constitute a very large part of the given beam, whereas in a purer beam the effect would be less significant. Furthermore, it can be observed in Fig. 6, that in the case of 0° (8.8 MeVcm^2/mg) the primary SEU cross section is in very good agreement with the experimental data, while at 60° (17.6 MeVcm^2/mg) it is higher than the experimental data of RADEF. This may be a result of the contribution of low energy ions generated by the lid of the memory, as the

memories tested at SPS-NA were still holding the original package, whereas those tested at RADEF were delidded.

As a conclusion, knowing and understanding the beam composition is very important for the data interpretation during UHE heavy ion test campaigns. In general, the UHE primary beam is the main contributor to SEEs, due to its higher LET. However, in cases of components with low threshold and a very contaminated beam, the secondaries could start playing a major role and affect the SEE measurement.

VII. Conclusions

In the present contribution, conclusions from the CERN UHE heavy ion test campaigns in 2017 and 2018 are presented. The main advantage of the UHE heavy ion beams is their long range. This introduces the possibility of in-air parallel board testing. In addition, the beam can arrive to the sensitive volume of the component without the need of delidding, and even in the most complex geometries, while preserving a constant LET, rendering UHE ions a very useful tool to SEE testing.

To further evaluate these beams, a thorough study on the purity of the heavy ion beam in one of the experiments has been performed. It has been demonstrated that in-beam elements, as well as the intervening air introduce a significant level of beam attenuation and fragmentation, despite the ion UHE. A careful beam analysis is, therefore, recommended prior to all heavy ion experiments, and the removal of any beam-intervening equipment is strongly suggested.

In the present study a quantification of the beam fragmentation through measurement and simulation was demonstrated, while the influence of the generated beam fragments on the SEE testing has been assessed. The main contributor to SEU generation was shown to be the primary UHE heavy ion beam, also in cases in which the percentage of the fragments is nonnegligible, when the threshold LET of the component is relatively high. In components with a very low LET threshold, possible fragments may affect the final result of the measure ment, and therefore, their percentage should be known.

Moreover, the possibility to test boards in parallel with UHE heavy ion beams has been confirmed, and a good understanding of the beam attenuation introduced has been achieved. The beam attenuation introduced by one PCB board was calculated as approximately 7.5%, and therefore, not a limiting factor to SEE testing. In all cases, however, the material budget between the primary beam and the tested boards should be narrowed as much as possible.

Furthermore, the fit parameters of a Weibull fit that matches the ESA monitor data acquired in very high energy and UHE heavy ions were calculated, while the experimental data follow this curve nicely.

Finally, no significant effect of UHE heavy ion beams in producing MBUs in SRAMs as a result of the broader and highly energetic ionization track was observed. Future works should include measurements with different components and more modern memory technologies to further examine this phenomenon, while longer irradiation times are also suggested.

References

[1] Test Procedures for the Measurement of SEE in Semiconductor Devices from Heavy-Ion Irradiation, *Standard JEDEC JESD57*, Addison-Wesley, Harlow, England, 1999.

[2] P. E. Dodd et al., "Impact of heavy ion energy and nuclear interactions on single-event upset and latchup in integrated circuits," *IEEE Trans. Nucl. Sci.*, vol. 54, no. 6, pp. 2303–2311, Dec. 2007.

[3] R. G. Alía et al., "Ultraenergetic heavy-ion beams in the CERN accelerator complex for radiation effects testing," *IEEE Trans. Nucl. Sci.*, vol. 66, no. 1, pp. 458–465, Jan. 2019.

[4] A. Virtanen, R. Harboe-Sorensen, H. Koivisto, S. Pirojenko, and K. Ranttila, "High penetration heavy ions at the RADEF test site," *in Proc. 7th Eur. Conf. RADiation Effects Compon. Syst. (RADECS)*, 2003, pp. 499–502.

[5] A. Virtanen, R. Harboe-Sorensen, A. Javanainen, H. Kettunen, H. Koivisto, and I. Riihimaki, "Upgrades for the RADEF facility," *in Proc. IEEE Radiat. Effects Data Workshop (REDW)*, 2007, pp. 38–41.

[6] Centre du Recherches du Cyclotron, Université Catholique de Louvain-la-Neuve, Belgium. Accessed: May 9, 2019. [Online]. Available: https://uclouvain.be/en/research-institutes/irmp/crc

[7] E. L. Petersen, V. Pouget, L. W. Massengill, S. P. Buchner, and D. McMorrow, "Rate predictions for single-event effects—Critique II," *IEEE Trans. Nucl. Sci.*, vol. 52, no. 6, pp. 2158–2167, Dec. 2005.

[8] B. D. Reddell et al., "Compendium of single event effects test results for commercial-off-the-shelf and standard electronics for low earth orbit and deep space applications," *in Proc. IEEE Radiat. Effects Data Workshop (REDW)*, Jul. 2017, pp. 57–65.

[9] V. Ferlet-Cavrois et al., "Influence of beam conditions and energy for SEE testing," *IEEE Trans. Nucl. Sci.*, vol. 59, no. 4, pp. 1149–1160, Aug. 2012.

[10] M. Bagatin et al., "Characterizing high-energy ion beams with PIPS detectors," IEEE Trans. Nucl. Sci., to be published.

[11] R. G. Alía et al., "LHC and HL-LHC: Present and future radiation environment in the high-luminosity collision points and RHA implications," *IEEE Trans. Nucl. Sci.*, vol. 65, no. 1, pp. 448–456, Jan. 2018.

[12] GSI Helmholtzzentrum für Schwerionenforschung. Accessed: May 8, 2018. [Online]. Available: https://www.gsi.de/en/work/research/appamml/plasmaphysicsphelix/infinfrastructatsis18hht.htm

[13] NASA Space Radiation Laboratory. Accessed: May 10, 2018. [Online]. Available: https://www.bnl.gov/nsrl/userguide/beam-ion-species-and-energies.php

[14] S. K. Hoeffgen et al., "Investigations of single event effects with heavy ions of energies up to 1.5 GeV/n," *IEEE Trans. Nucl. Sci.*, vol. 59, no. 4, pp. 1161–1166, Aug. 2012.

[15] P. F. Martinez et al., "SEE tests with ultra energetic Xe ion beam in the CHARM facility at CERN," *IEEE Trans. Nucl. Sci.*, vol. 66, no. 7, pp. 1523–1531, Jul. 2019, doi: 10.1109/TNS.2019.2907112.

[16] A. Infantino et al., "Dose gradient assessment at the new CERN CHARM irradiation facility," *Radiat. Phys. Chem.*, vol. 155, pp. 225–232, Feb. 2019.

[17] J. Mekki et al., "CHARM: A mixed field facility at CERN for radiation tests in ground, atmospheric, space and accelerator representative environments," *IEEE Trans. Nucl. Sci.*, vol. 63, no. 4, pp. 1–9, Jul. 2016, doi: 10.1109/TNS.2016.2528289.

[18] A. Thornton, "CHARM facility test area radiation field description," CERN, Geneva, Switzerland, Tech. Rep. CERN-ACC-NOTE-2016-12345. [Online]. Available: https://cds.cern.ch/record/2159238.

[19] R. Harboe-Sorensen et al., "PROBA-II technology demonstration module in-flight data analysis," *IEEE Trans. Nucl. Sci.*, vol. 59, no. 4, pp. 1086–1091, Aug. 2012.

[20] R. Harboe-Sorensen et al., "From the reference SEU monitor to the technology demonstration module on-board PROBA-II," *IEEE Trans. Nucl. Sci.*, vol. 55, no. 6, pp. 3082–3087, Dec. 2008.

[21] R. Harboe-Sorensen et al., "The technology demonstration module on-board PROBA-II," *IEEE Trans. Nucl. Sci.*, vol. 58, no. 3, pp. 1001–1007, Jun. 2011.

[22] C. Poivey, "Update on PROBA-2 TDM and ALPHASAT TDP8 flight data," *in Proc. SEE Symp.*, 2016.

[23] A. Ferrari, P. R. Sala, A. Fassò, and J. Ranft, FLUKA: A Multi-Particle Transport Code (Program Version 2005). Geneva, Switzerland: CERN, 2005.

[24] T. T. Böhlen et al., "The FLUKA code: Developments and challenges for high energy and medical applications," *Nucl. Data Sheets*, vol. 120, pp. 211–214, Jun. 2014.

[25] C. Cazzaniga, R. G. Alía, M. Kastriotou, M. Cecchetto, P. Fernandez-Martinez, and C. D. Frost, "Study of the deposited energy spectra in silicon by high energy neutron and mixed fields," *IEEE Trans. Nucl. Sci.*, to be published.

[26] J. A. Scheer, "Pulse shape discrimination with solid state detectors," *Nucl. Inst. Meth.*, vol. 22, pp. 45–47, Mar. 1963.

[27] P. Kavrigin et al., "Pulse-shape analysis for gamma background rejection in thermal neutron radiation using CVD diamond detectors," *Nucl. Instrum. Methods Phys. Res. A, Accel. Spectrom. Detect. Assoc. Equip.*, vol. 795, pp. 88–91, Sep. 2015.

[28] B. K. Nayak, E. T. Mirgule, and R. K. Choudhury, "Application of pulse shape discrimination in Si detector for fission fragment angular distribution measurements," *Pramana*, vol. 65, no. 6, pp. 1053–1059, 2005.

[29] C. Cazzaniga et al., "Measurements of ultra-high energy lead ions using silicon and diamond detectors," Rutherford Appleton Lab., ISIS Facility, STFC, Didcot, U.K., Tech. Rep.

[30] J. F. Ziegler, M. D. Ziegler, and J. P. Biersack, "SRIM—The stopping and range of ions in matter (2010)," *Nucl. Instrum. Meth. Phys. Res. B, Beam Interact. Mater. At.*, vol. 268, pp. 1818–1823, Jun. 2010. [Online]. Available: https://ui.adsabs.harvard.edu/abs/2010NIMPB.268.1818Z

[31] R. Brun and F. Rademakers, "ROOT—An object oriented data analysis framework," *Nucl. Instrum. Meth. Phys. Res. A, Accel. Spectrom. Detect. Assoc. Equip.*, vol. 389, pp. 81–86, Apr. 1997. [Online]. Available: http://root.cern.ch/

[32] R. G. Alía et al., "Sub-LET threshold SEE cross section dependency with ion energy," *IEEE Trans. Nucl. Sci.*, vol. 62, no. 6, pp. 2797–2806, Dec. 2015.

[33] R. G. Alía et al., "Direct ionization impact on accelerator mixed-field soft error rate," *IEEE Trans. Nucl. Sci.*, to be published.

[34] M. Tali, "Single-event radiation effects in hardened and state-of-the-art components for space and high-energy accelerator applications," *Ph.D. dissertation, Dept. Math. Sci., Univ. Jyväskylä*, Jyväskylä, Finland, 2019. [Online]. Available: http://urn.fi/URN:ISBN:978-951-39-7794-8